# Supporting Information

## Ultrahigh energy harvesting properties in temperature insensitive eco-friendly high performance KNN-based textured ceramics

*Jinfeng Lin[a], Yingbo Cao[a], Kun Zhu[a], Fei Yan[a], Cheng Shi[a], Hairui Bai[a], Guanglong Ge[a], Jing Yang[a], Weiwei Yang[b], Yunjing shi[a], Guohui Li[a], Huarong Zeng[b], Jiwei Zhai[a,]**

[a] *Key Laboratory of Advanced Civil Engineering Materials of Ministry of Education, Functional Materials Research Laboratory, School of Materials Science and Engineering, Tongji University, Shanghai, 201804, China*

[b] *CAS Key Laboratory of Inorganic Functional Materials and Devices, Shanghai Institute of Ceramics, Chinese Academy of Sciences, Shanghai 201899, China*

***Corresponding author.***

***E-mail address:*** *apzhai@tongji.edu.cn*

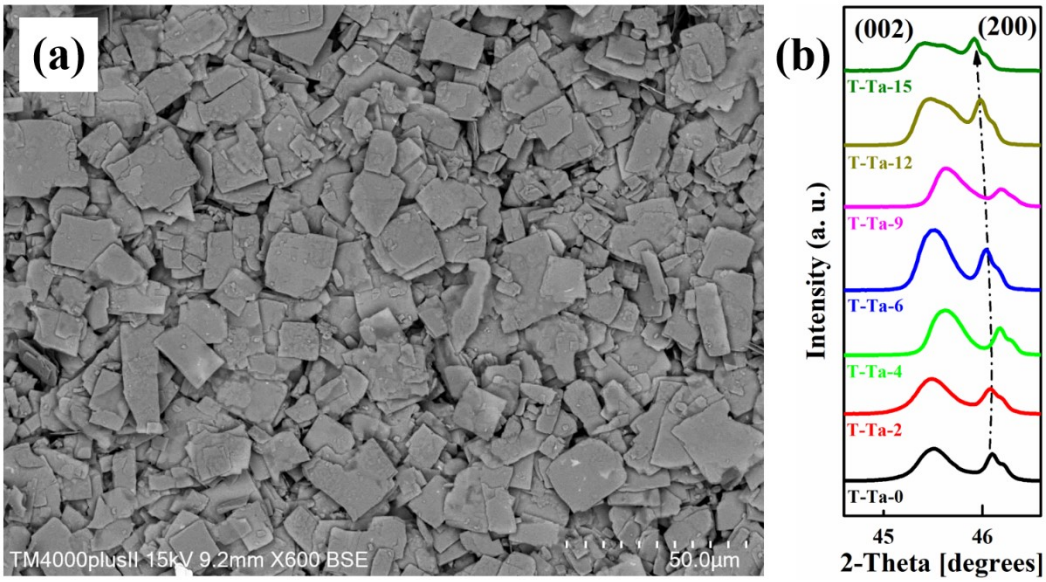


**Figure S1.** (a) The SEM of the NN platelet template; (b) The details of XRD patterns of the texture ceramics around 45°.

It is well known that the texture degree of the KNN-based textured ceramics is severely affected by the quantity and quality of the added NN template, the complexity of the phase composition, the sintering temperature, the holding time as well as the tape casting process. For the same O-T phase coexistence, the texture degree ($f_{(00l)}$) of the KNNTa-BNN ceramics is higher than the previous experimental results,[1,2] which is inseparable from the added high-quality NN platelet template and its suitable content (4 wt.%).

It is well known that the piezoelectric performance of KNN-based ceramics is especially sensitive to the perovskite phase structure, which can be quantified by assessing relative intensities of (002) and (200) peaks.[3] As x increases from 0 to 15, the intensity of the (200) peak gradually increases, indicating that the content of the T phase of both of the random and texture ceramics gradually increases, which is consistent with the result of Raman spectroscopy and the temperature-dependent dielectric

constants and losses (Fig. S3). When x = 15, the (200) peak intensity of the texture ceramic exceeds (002), indicating the transition from O phase dominance to T phase dominance (Fig. S1b).

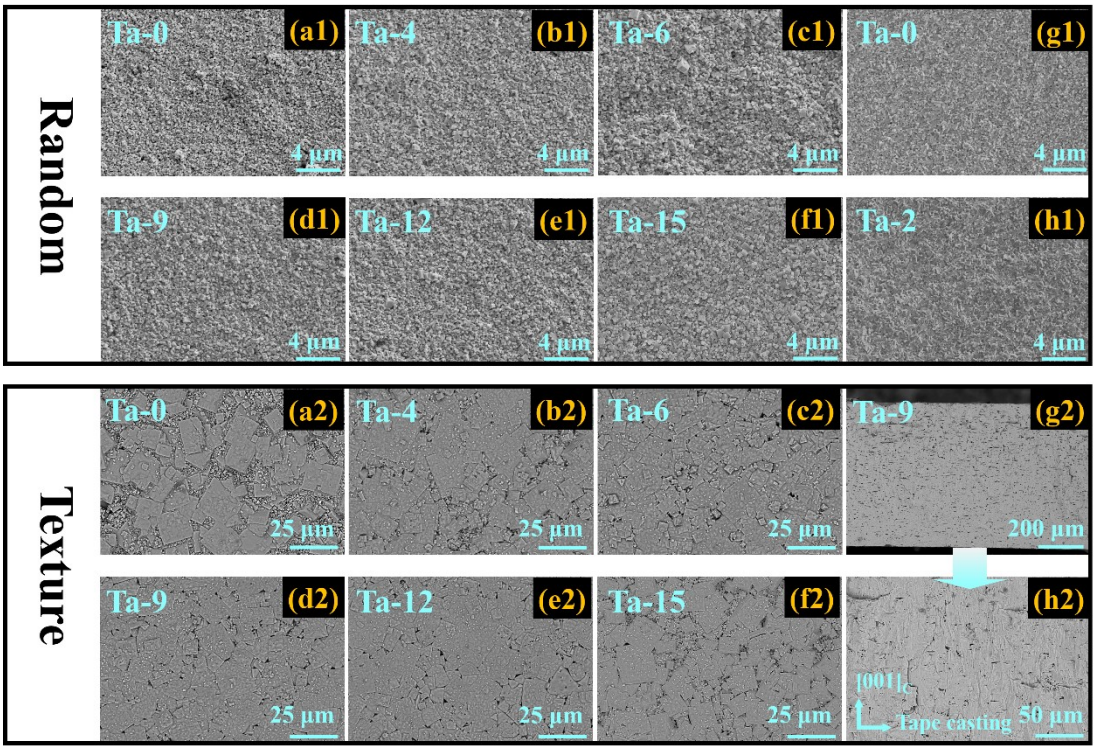


**Figure S2.** The free surface SEM images of the random (a1-f1) and texture (a2-f2) ceramics; The cross-sectional SEM images of the random (g1-h1) and (g2-h2) texture ceramics.

It is found that initial nucleation of textured grains at template-matrix interface begins at ~850°C, accelerating as temperature increases, templates and matrix react via inter-diffusion.[4] Therefore, as the holding time increases, the KNN matrix powder grows along the template so that the thickness and width of the template gradually increase, and finally large-sized oriented grains are formed, which are much larger than that of random ceramics.

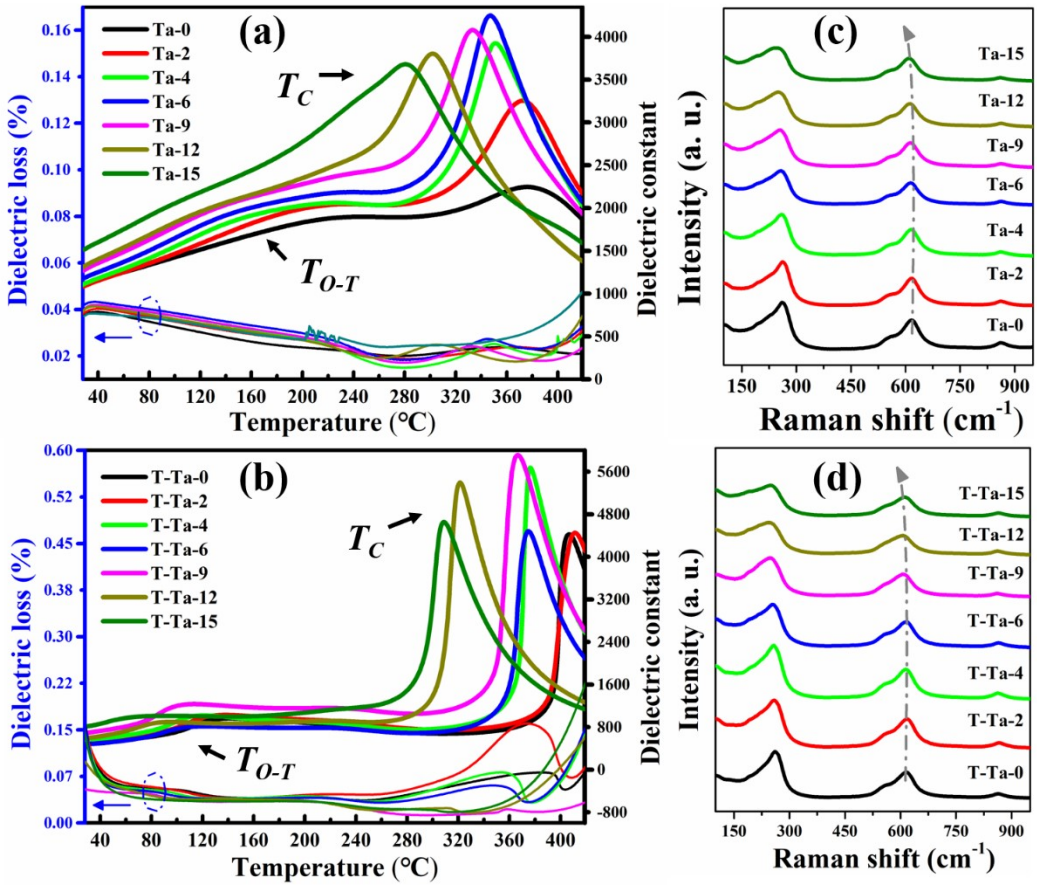


**Figure S3.** Temperature-dependent dielectric constants and losses curves of the random (a) and texture (b) ceramics; Room temperature Raman spectrum of the random (c) and texture (d) ceramics.

On the one hand, there are more PNRs exist in the random ceramics, which are less stable than the large-scale long-range ferroelectric domains of the textured ceramics, hence, its Curie temperature is lower than that of the textured ceramics. On the other hand, the presence of PNRs makes the $T_{O-T}$ and $T_{R-O}$ of the random ceramics more relaxor, which dielectric peaks are dispersed and broadened, and requiring a certain relaxation time during phase transition, thus presenting a higher phase transition temperature (Fig. S6). Therefore, the textured ceramics exhibit higher $T_C$ and lower $T_{R-O}$ and $T_{O-T}$.[5,6]

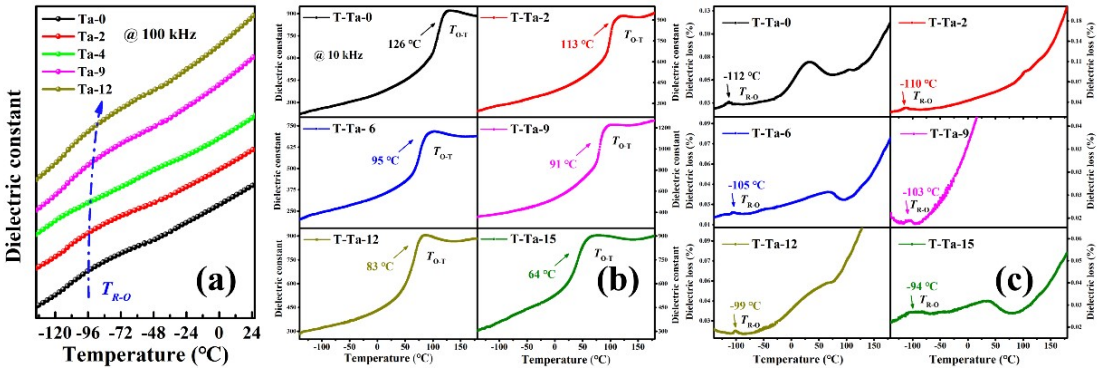


**Figure S4.** Temperature-dependent dielectric constants and losses at low temperature of the random (a) and texture (b, c) ceramics.

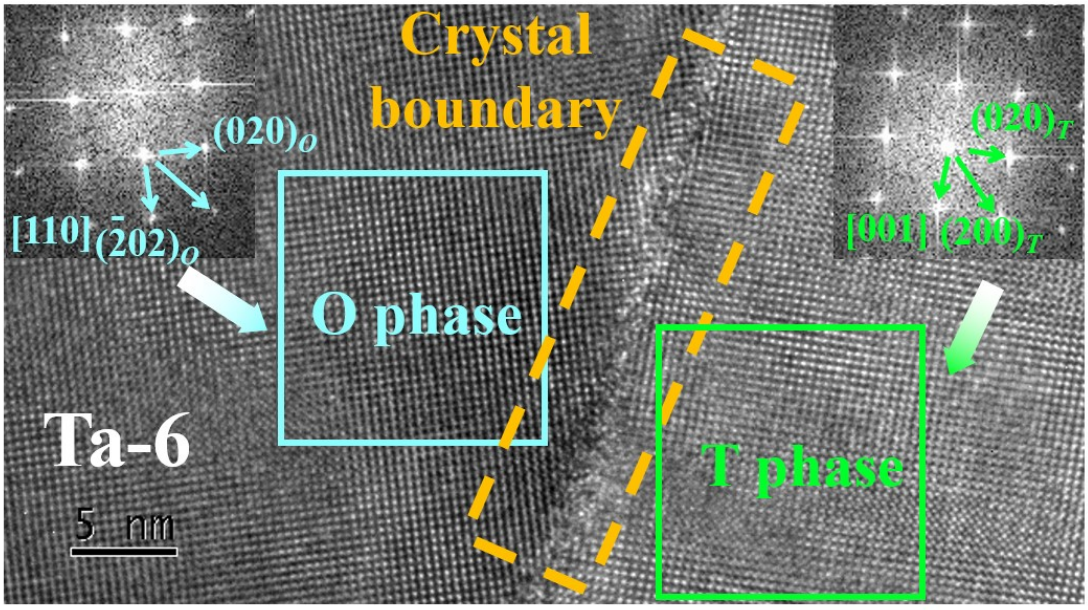


**Figure S5.** High-resolution TEM and the corresponding diffraction patterns of the Ta-6.

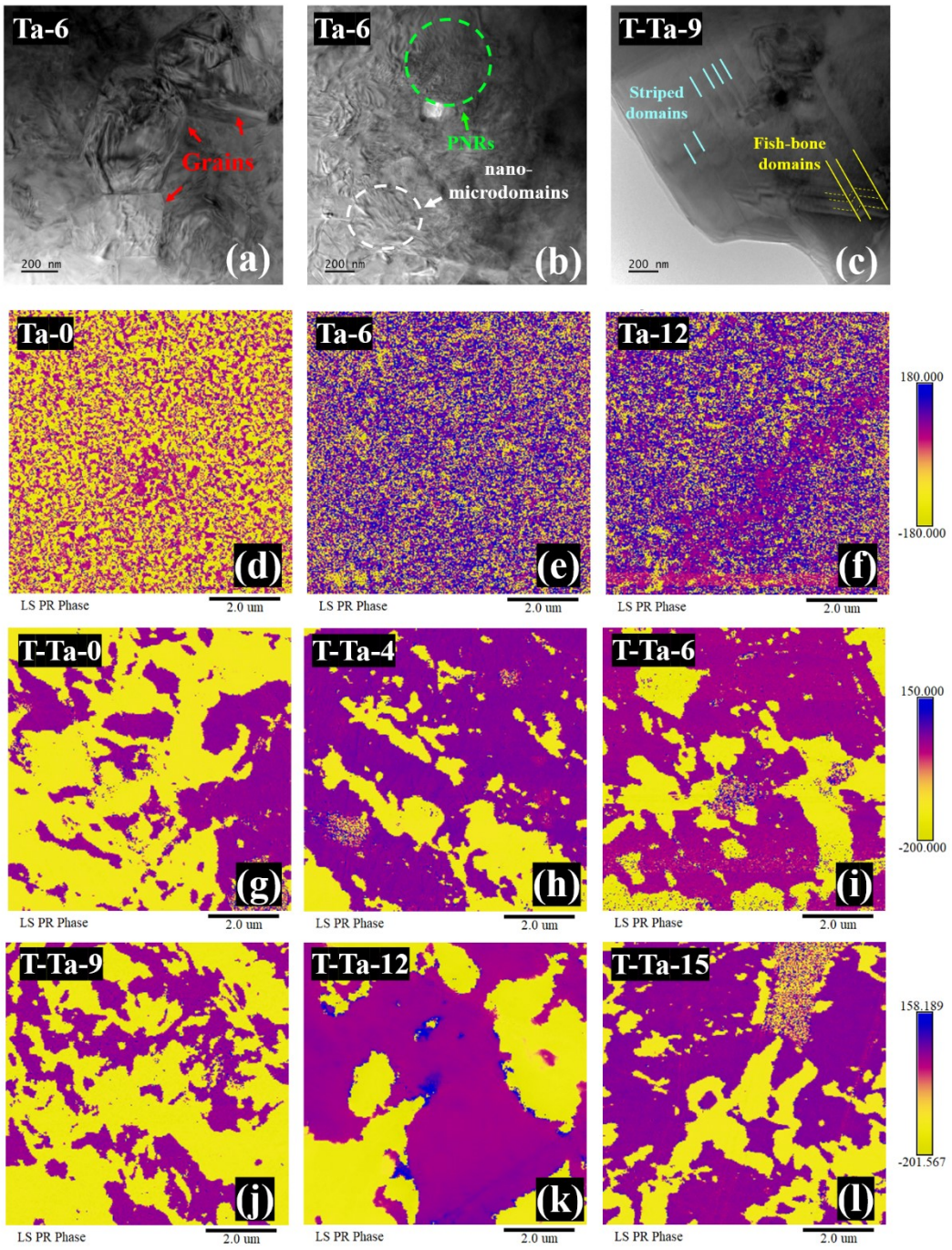


**Figure S6.** TEM images of Ta-6 (a, b) and T-Ta-9 (c); PFM phase images of the random (d-f) and texture (g-l) ceramics.

As shown in Fig. 3a and Fig. S6a and b, the fine grains (< 0.4 μm) accompanied by an abundance of nano-microdomains and polar nanoregions (PNRs) can be seen in the random ceramics (i.e., Ta-6). In contrast, except for the few remaining nano-

microdomains (Fig. 3d), various large-scale domains with regular morphology can be seen in the texture ceramics (i.e., T-Ta-9), including parallel strip-shaped domains (180°) in the size range of 0.5-2.5 μm, fish-bone domains (45°) and large-area labyrinth domains (90°) (Figs. 3b-d, 5c and Fig. S6c), which are attributed to the large-sized $<00l>_C$ oriented grains, thereby improving the piezoelectric properties of texture ceramics.

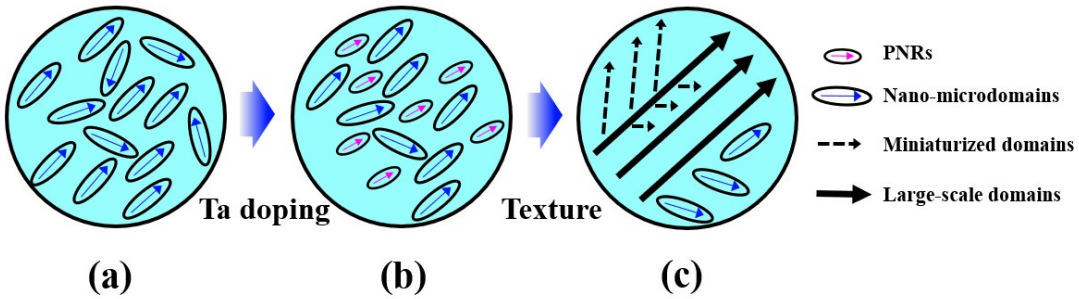


**Figure S7.** Schematic diagram of the domain structure evolution for (a) KNN-BNN matrix, (b) KNNTa-BNN random ceramics and (c) KNNTa-BNN texture ceramics.

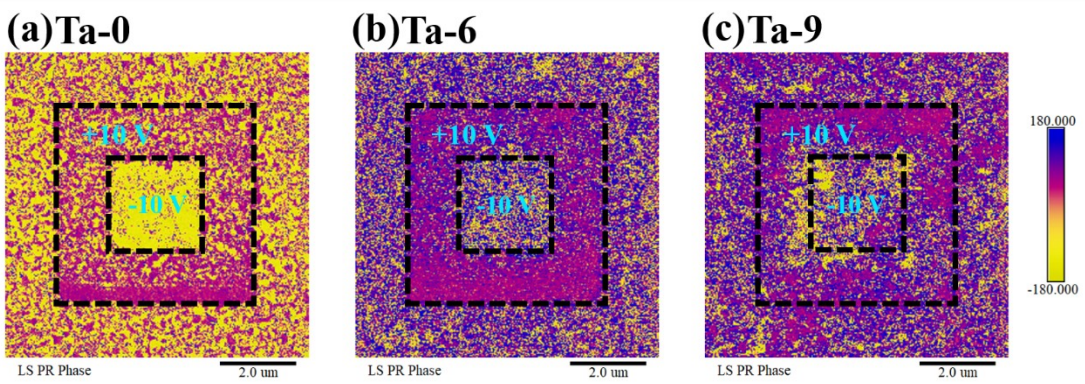


**Figure S8.** Poling patterns in PFM phase images of (a) Ta-0, (b) Ta-6 and (c) Ta-9 via applying +10 V/-10 V DC tip biases.

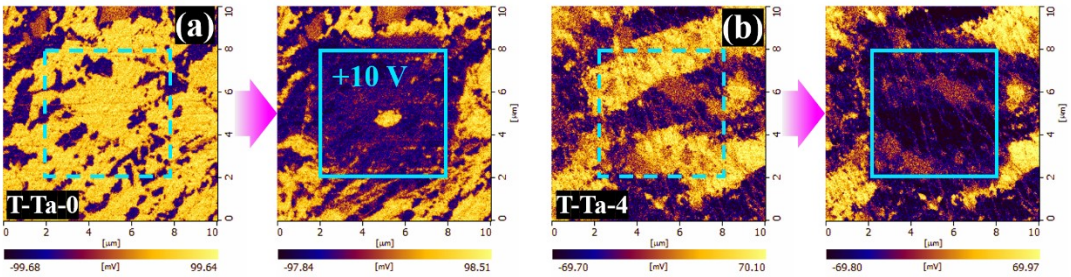


**Figure S9.** Poling patterns in PFM phase images of T-Ta-0 (a) and T-Ta-4 (b) via applying +10 V DC tip biases.

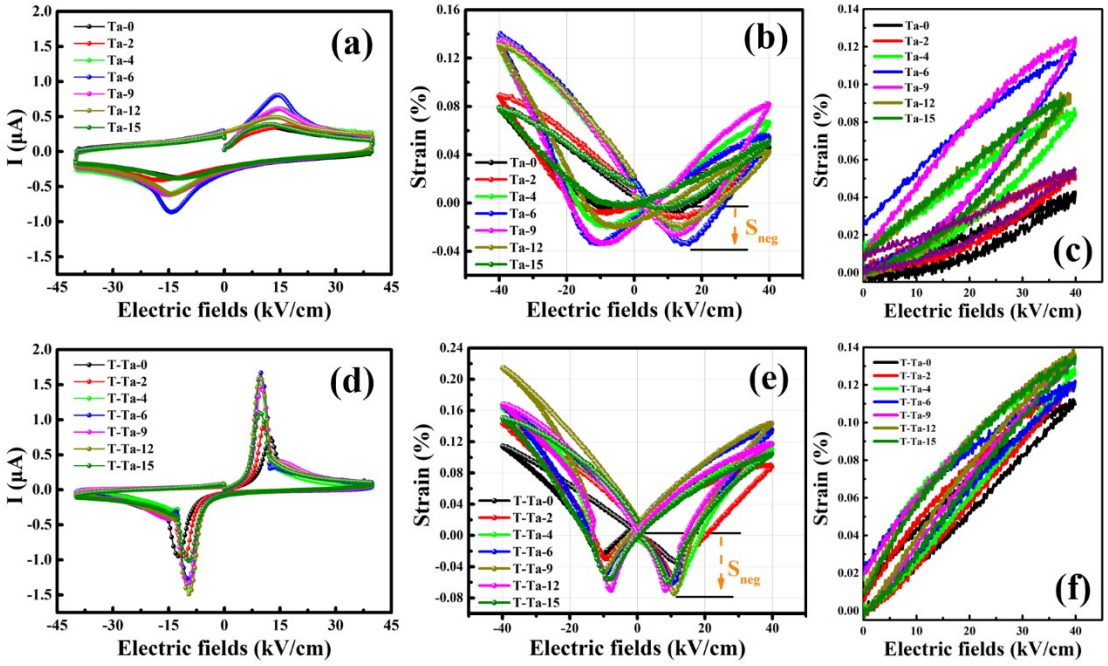


**Figure S10.** *I-E* loops, bipolar strain curves and unipolar strain curves and of the random (a-c) and texture (d-f) ceramics.

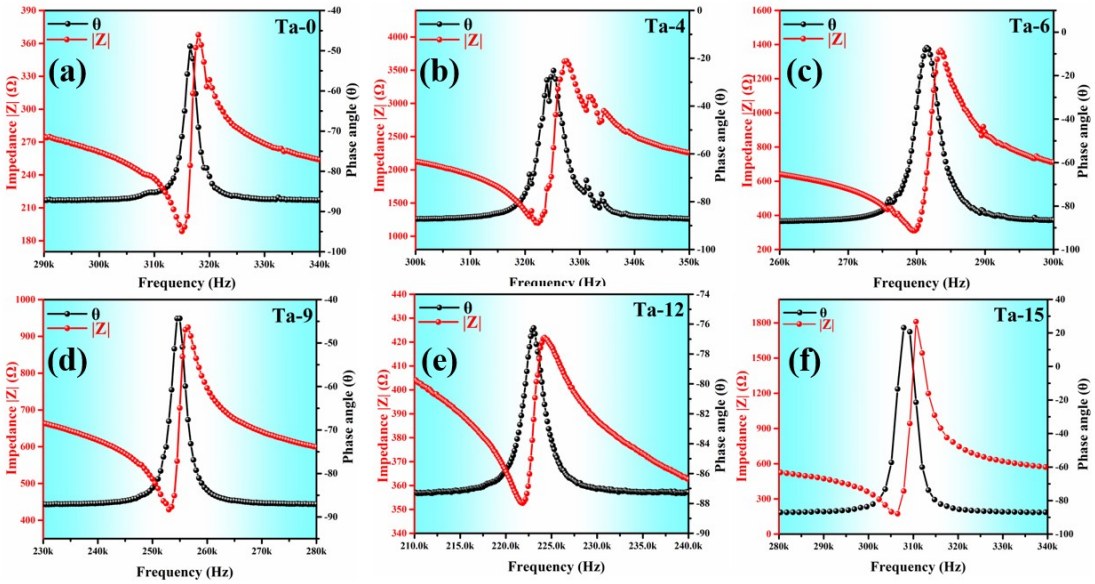


**Figure S11.** (a-f) Impedance Z and phase angle θ against frequency of the random ceramics measured at room temperature.

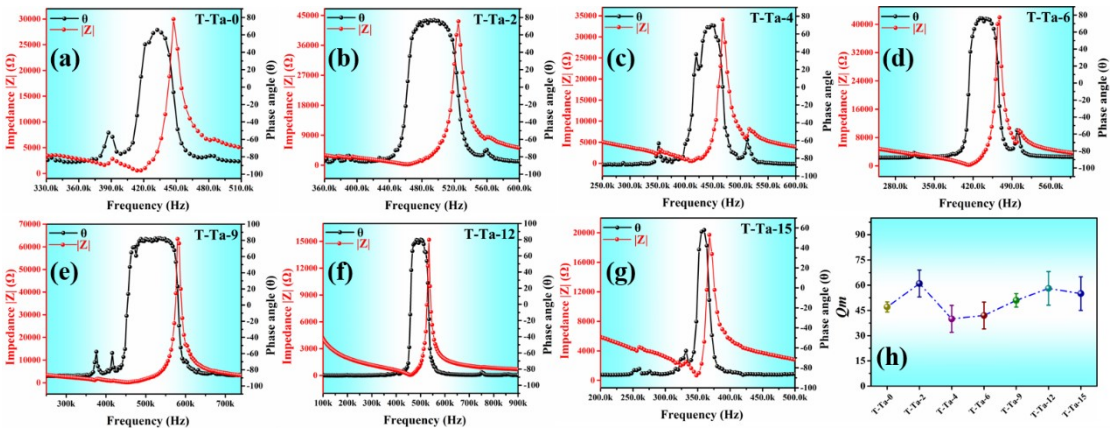


**Figure S12.** (a-g) Impedance Z and phase angle θ against frequency and (h) the calculated $Q_m$ of the texture ceramics measured at room temperature.

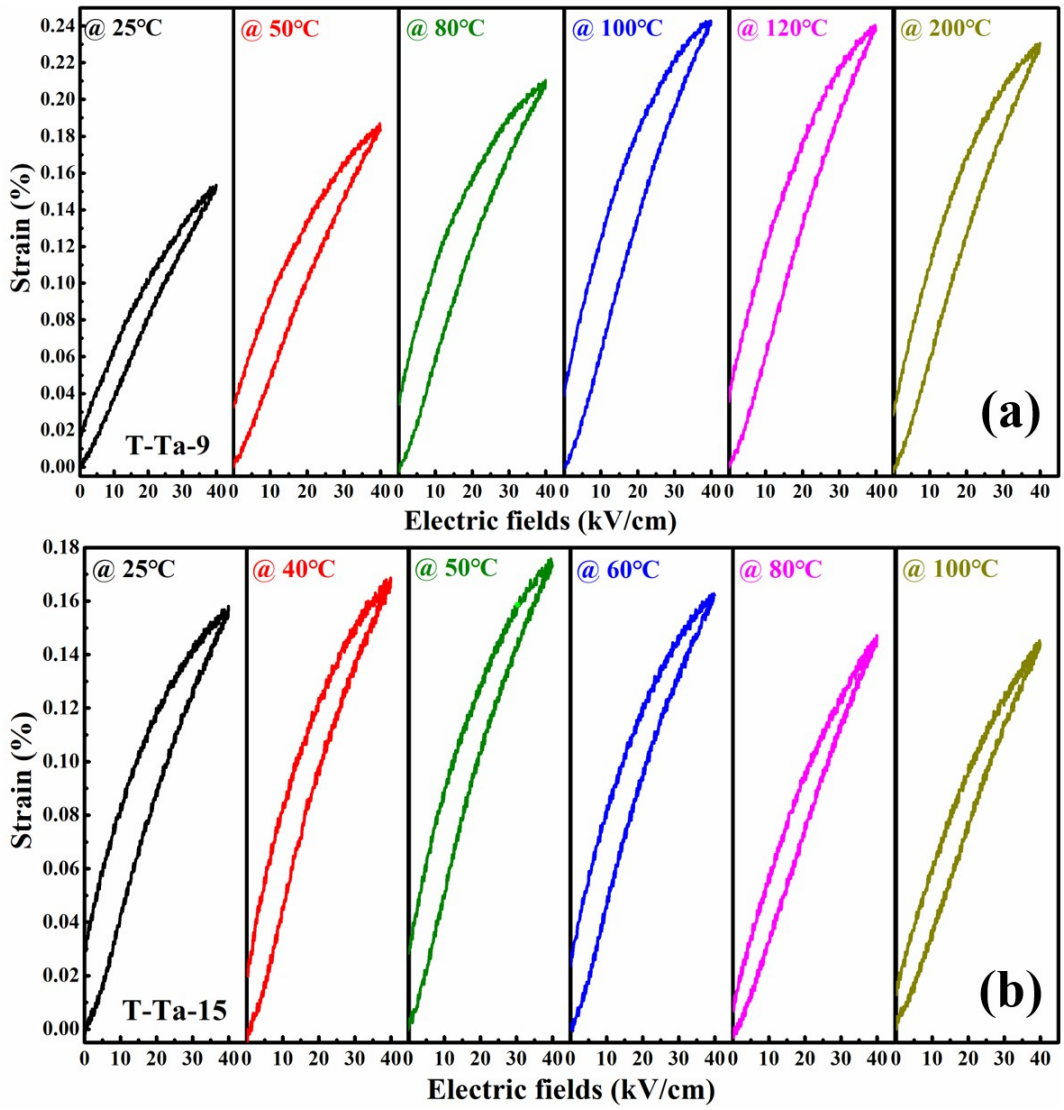


**Figure S13.** *In-situ* temperature-dependent unipolar strain curves of (a)T-Ta-9 and (b) T-Ta-15.

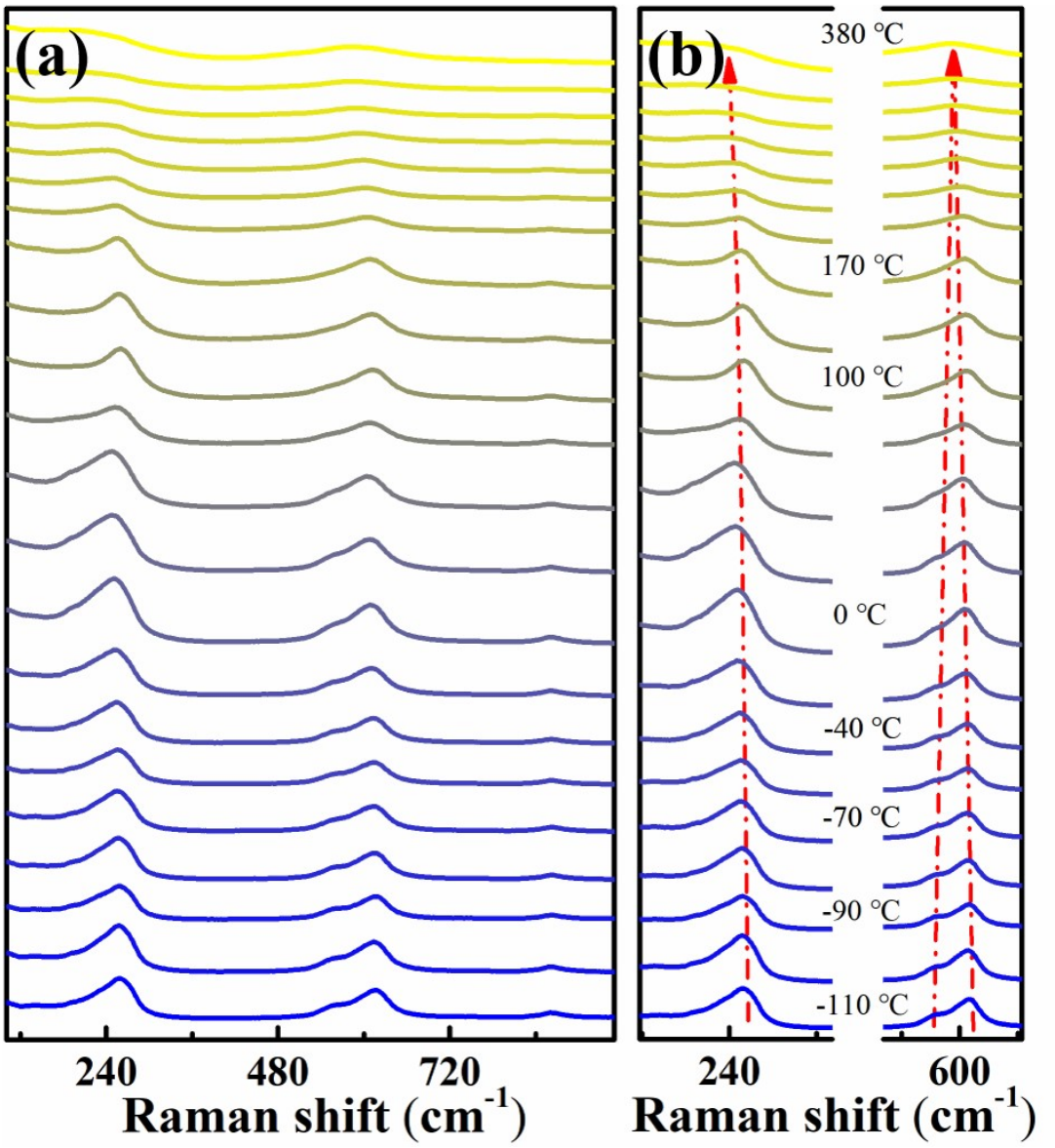


**Figure S14.** (a) *In-situ* variable temperature Raman spectrum for T-Ta-9; (b) The corresponding enlarged details of *In-situ* variable temperature Raman spectrum around 200 $cm^{-1}$ and 600 $cm^{-1}$.

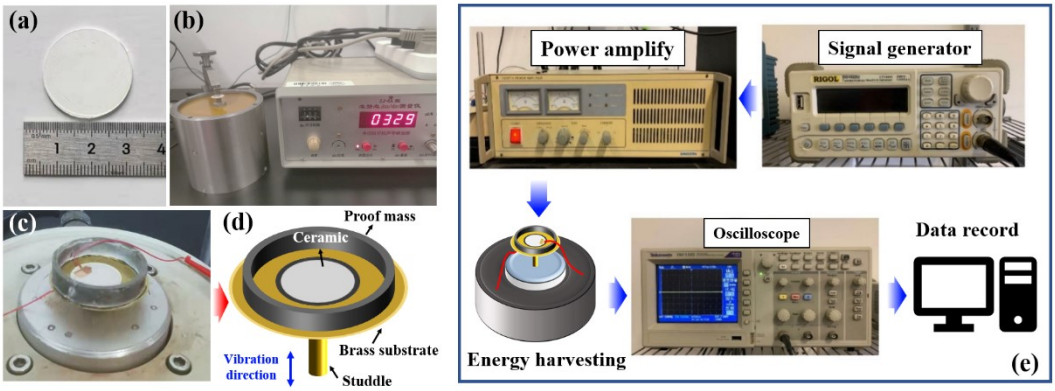


**Figure S15.** Partial preparation process of the T-Ta-9 PCD vibration energy harvester (a), and the corresponding test system (b).

## References

1. B.H. Liu, P. Li, B. Shen and J.W. Zhai, *Ceram. Int.* 2017, **43**, 8004-8009.

2. B.H. Liu, P. Li, B. Shen and J.W. Zhai, *J. Am. Ceram. Soc.* 2018, **101**, 265-273.

3. K. Wang, F.-Z. Yao, W. Jo, D.K. Gobeljic, V. V. Shvartsman, D. C. Lupascu, J.-F. Li and J.G. Rödel, *Adv. Funct. Mater.* 2013, **23**, 4079-4086.

4. A.D. Moriana and S.J. Zhang, *J. Materiomics* 2018, **4**, 277-303.

5. Z.Y. Liu, H.Q. Fan, Y.W. Zhao and G.Z. Dong, *J. Am. Ceram. Soc.* 2016, **99**, 146–151.

6. M.J. Kosec, V. Bobnar, M. Hrovat, J. Bernard, B. Malic and J. Holc, *J. Mater. Res*. 2004, **19**, 1849-1854.